THE AMERICAN SOCIETY OF MECHANICAL ENGINEERS
345 E. 47th St., New York, N.Y. 10017

97-GT-69

An Investigation of Effectiveness and Heat Transfer on a Showerhead-Cooled Cylinder

A. Hoffs
ABB Power Generation Ltd.
Gas Turbine Development
Baden, Switzerland

U. Drost, A. Bölcs
Swiss Federal Institute of Technology
EPFL-LTT
Lausanne, Switzerland

ABSTRACT

An investigation of effectiveness and heat transfer on a cylinder model with showerhead cooling has been conducted in a free jet test facility, using the transient liquid crystal technique. A three- and a four-row configuration, covering a region of ±21°, were chosen to study the cooling behaviour for zero and off-design incidences. Typical engine airfoil leading edge conditions were maintained for the freestream Reynolds and Mach numbers to 1.55e5 and 0.26 for the three-row, and 1.84e5 and 0.30 for the four-row configuration, at a turbulence intensity of 7%. The blowing and momentum rates were varied from 0.4 to 1.8 and 0.1 to 1.9, at a density ratio of 1.65. At zero incidence it could be observed for both configurations that the highest effectiveness of about 0.3 was achieved at a blowing rate of 0.4. Negative incidence for the four-row configuration resulted in much higher effectiveness, being as high as 0.5 at a blowing rate of 0.9, with an associated high heat transfer. Much lower effectiveness was achieved at positive incidence, where the blowing rate of 0.9 showed the best cooling behaviour. Higher effectiveness—but also increased heat transfer—was in general observed for the four-row configuration, with a 60% higher massflow.

NOMENCLATURE

c_p	specific heat capacity, J/kgK
c_p	non-dimensional pressure, $(p-p_1)/(0.5*\rho_1 u_1^2)$
CD	discharge coefficient
D	cylinder diameter, mm
DR	coolant-to-gas density ratio, ρ_c/ρ_g
d	hole diameter, mm
G	blowing rate, $\rho_c u_c/\rho_g u_g$
I	momentum flux ratio, $\rho_c u_c^2/\rho_g u_g^2$
l	cooling hole length, mm
M	Mach number
Me	grid mesh size, mm
Nu	Nusselt number
p	hole pitch, mm
Re	Reynolds number
$R_{z,t,a}$	surface roughness DIN4768
T	temperature, K
t	time, s
Tu	turbulence intensity, %
y	coordinate normal to model surface, mm

Greek letters

α	heat transfer coefficient, W/m²K
α	streamwise hole injection angle, °
β	lateral hole injection angle, °
η	film cooling effectiveness, $(T_{rg}-T_{aw})/(T_{tg}-T_{tc})$
λ	heat conduction coefficient, W/mK
Λ	thermal diffusivity, m²/s
φ	cylinder angle, °
ρ	density, kg/m³
θ	non-dimensional temperature, $(T_{tg}-T_{tc})/(T_{rg}-T_w)$

Indices

1	approach conditions
aw	adiabatic wall
D	with respect to cylinder diameter
f	with film cooling
i	initial
g	free stream
p	plenum
r	recovery
t	total
w	wall

INTRODUCTION

The power output and efficiency level of a gas turbine improves by increasing the turbine inlet temperature. Since these temperatures exceed the maximum allowable blade material temperature the airfoils have to be cooled to achieve safe operating conditions. Hence, knowledge of the detailed heat transfer characteristics is required for the design of

Presented at the International Gas Turbine & Aeroengine Congress & Exhibition
Orlando, Florida — June 2–June 5, 1997

airfoils which have to operate for a certain guaranteed number of hours without failure.

The leading edge of an airfoil is extremely exposed to the hot gas flow, resulting in high heat transfer coefficients. A common technique to protect this region is to pass cooling air through elaborate internal convective schemes in order to lower the blade material temperature. This cooling air can also be used for film cooling, where the secondary air is ejected through rows of closely spaced discrete holes. The effect is an additional convective cooling close to the holes, and the formation of a protective layer on the surface effecting the region further downstream. Mayle and Anderson (1989) reasoned that a simple one-dimensional heat transfer model shows that most of the overall cooling effect results from the convective pickup in the holes, and describe the film as a bonus effect. As the injection process disturbs the character of the boundary layer it is also important to judge on the effect of this alteration. Unlike for film cooling on a flat plate, the stagnation film cooling contains the additional aspects of a highly accelerated flow with a thin boundary layer, and a coolant injection at angles almost opposite to the approaching main flow.

Recent work on showerhead cooling has concentrated on models with rather large spacing of rows. Mick and Mayle (1988) conducted investigations on the circular leading edge of a blunt body with rows at ±15° and 44°. They concluded that for typical turbine temperatures film cooling at the leading edge generally reduces the heat load—provided that the correct blowing rate is used. Salcudean et al. (1994) chose a similar film cooling geometry and showed that the relative stagger of the two rows was an important parameter, as an ideal interaction between the two rows should result in a complete coverage of the downstream surface. Mehendale and Han (1990) used a large blunt body with a cylindrical leading edge and cooling rows at ±15° and ±40° to investigate the influence of high freestream turbulence. The results indicated that the film effectiveness decreased with increasing blowing ratio, with an inverse effect for the heat transfer coefficient. As opposed to the present study these tests were conducted with a constant heat flux surface. High turbulence had a significant influence on the film effectiveness at a low blowing ratio of 0.4, while this effect diminished at higher blowing ratios. A study of convective heat transfer around a film-cooled turbine blade with leading edge film cooling was conducted by Camci and Arts (1990) in a short-duration facility, using thin film gauges. A three-row configuration was employed with holes at the stagnation point and at ±42°. It was found that leading edge film cooling was quite effective for low blowing rates. The freestream turbulence was varied between 0.8 to 5.2% at constant film cooling parameters, and no significant effect was identified.

Karni and Goldstein (1990) varied the injection location relative to the stagnation line to investigate the cooling behavior of one single row at different blowing rates between 0.5 and 2.0, which corresponds to the range investigated in the present work. Among other results it was reported that the mass transfer distribution was extremely sensitive to small changes in the injection hole location relative to the stagnation point. This was especially remarked for cooling on the stagnation line, which can be confirmed by the present authors for the tests on the three-row configuration.

Present investigation

In the present work, effectiveness and heat transfer have been investigated on a cylinder model with showerhead cooling, for a three- and a four-row configuration at zero and off-design incidences. Typical engine airfoil leading edge conditions were maintained for the freestream Reynolds and Mach numbers to 1.55e5 and 0.26 for the three-row, and 1.84e5 and 0.30 for the four-row configuration, at a turbulence intensity of 7%. The blowing and momentum rates were varied from 0.4 to 1.8 and 0.1 to 1.9 (based on approach conditions), to cover a reasonable range of coolant massflow. The density ratio of 1.65 was obtained with the foreign gas CO_2 to simulate the heavier coolant at low temperature. The cooling rows covered only a region of ±21°, thus having a much smaller spacing than the ones reported in the literature. Both film cooling effectiveness and heat transfer were determined by conducting several tests at identical flow conditions but different coolant temperatures, using the transient liquid crystal technique.

TEST FACILITY/MEASURING EQUIPMENT

Wind tunnel

The experiments were conducted in a free jet test facility which was supplied by a continuously running compressor. The diameter of the free jet is 150 mm and has a sharp-edged exit which holds a square-meshed turbulence grid (with a meshsize Me=15 mm and a barsize b=3 mm). The cylinder was placed at a distance of x/Me=10 where a turbulence intensity of 7% and a lengthscale of 13 mm were measured with a single hot-wire probe (Drost et al., 1997).

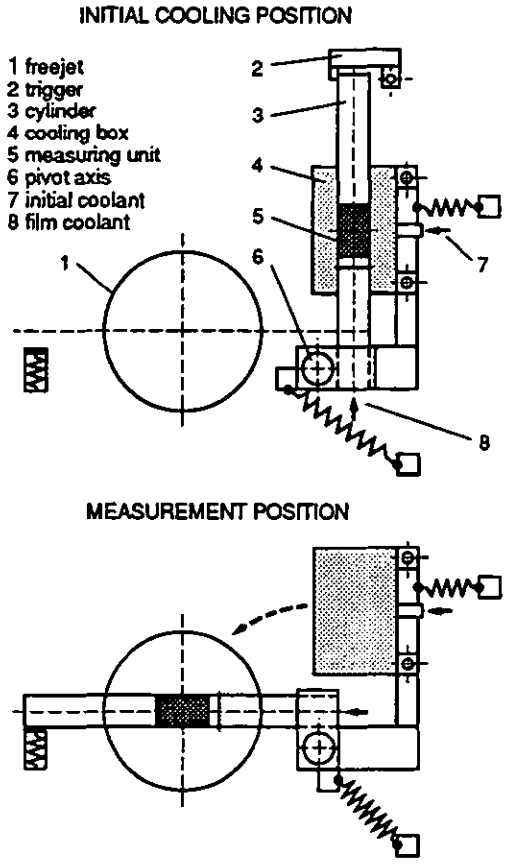

Fig. 1 Cylinder insertion system

Cylinder insertion system

The use of a transient measurement technique for the investigation required a sudden temperature step for the test model. For this purpose, a cylinder insertion system was newly developed—based on a former construction where the cylinder was pivoted around an axis into the mainstream (Häring et al., 1995). For the showerhead cooling tests, initial pre-cooling of the measurement section below ambient temperature was necessary. The new design allowed instantaneous insertion of the cylinder into the free jet while providing the possibility to precondition the measurement section of the cylinder (Fig. 1).

For pre-conditioning the cylinder is placed in its vertical position with the cooling box enclosing the measurement section of the cylinder. Cooling air is supplied by an external cooling device and blown onto the measuring section through a fine gauze to obtain an even temperature distribution. The box is divided into two parts and guided on axes which can be uncoupled from the cylinder movement. The two parts of the box are forced together by means of a clamp since both parts are connected to springs pulling in the opposite direction. The mechanism is triggered when the desired uniform initial temperature is reached, then both the cylinder and the box pivot towards the flow field. After approximately one third of the rotation movement the clamp releases and the cooling box opens abruptly. The cylinder is uncovered and falls into the flow field while the cooling box is pulled back so as not to disturb the flow. The cylinder movement is enforced by two springs to achieve a fast and repetitive movement—obtaining insertion times of below 0.1 s. The far end of the cylinder falls into a damping mechanism to avoid breakage of the cylinder. The bypass valve for the showerhead cooling fluid is coupled with the insertion of the cylinder via a mechanic switch and an electronic signal.

Cylinder model

The cylinder model (Fig. 2) has a showerhead measurement unit out of Plexiglas of a width of 60 mm to obtain a two-dimensional coolant ejection, which was made interchangeable for different geometries. Steady state thermocouples were placed into and next to the showerhead unit to measure the initial temperature and to conduct the liquid crystal calibration. Static pressure tappings could only be placed over about 180° close to the measurement region. For the plenum chamber the largest possible diameter was used to obtain as low a velocity as possible. Two transient thermocouples and a static pressure tapping were located behind the coolant holes, while a fine gauze was installed upstream to help mix the fluid. A flexible tube with a heat exchanger was used to connect the coolant supply and the bypass valve. Care was taken to obtain a good sealing of all coolant supply connections in order to prevent any massflow leakage.

The showerhead cooling geometries consisted of a three- and a four-row configuration in staggered arrangement. The different geometrical parameters are listed in table 1.

cylinder	rows [°]	α [°]	β [°]	p/d [-]	l_h/d [-]
3-row	-21/0/+21	90	45	6.3	4.7
4-row	-21/-7/+7/+21	90	45	5.0	4.7

Table 1 Showerhead cooling configuration data

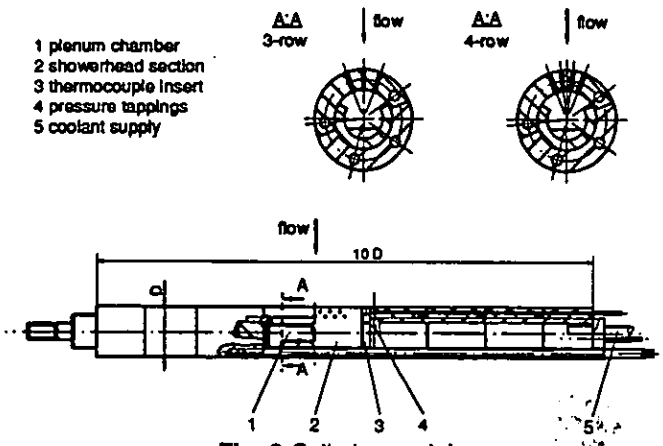

Fig. 2 Cylinder model

Theory

The local heat flux in the film cooling situation can be described as follows,

$$q = \alpha_f (T_{aw} - T_w) \tag{1}$$

where the convection coefficient is based on the unknown adiabatic wall temperature, being a function of the supply temperatures of the main and secondary streams and the degree of mixing. In dimensionless form this temperature becomes the film cooling effectiveness, defined for flow with dissipation as (Teekaram et al., 1990),

$$\eta = \frac{T_{aw} - T_{rg}}{T_{tc} - T_{tg}} \tag{2}$$

The two unknowns of such a three-temperature situation are thus the heat transfer coefficient α_f and the film cooling effectiveness, η. Both values are functions of the aerodynamic character of the flow field alone (Vedula and Metzger, 1991).

The effectiveness and heat transer measurements have been conducted with the transient liquid crystal technique. The technique requires a uniform initial temperature of the model which is rapidly exposed to a flow at a different temperature for a limited amount of time. It is assumed that within the testing time the penetration of the heating pulse into the model is small compared to the model wall thickness. Thus, the heat conduction can be considered to be unsteady and one-dimensional in a semi-infinite material. The governing differential equation and appropriate boundary conditions are then,

$$\frac{\partial^2 T}{\partial y^2} = \frac{1}{\Lambda} \frac{\partial T}{\partial t} \tag{3}$$

$$\lim_{y \to \infty} T(y,t) = T_i \tag{4}$$

$$T(y,0) = T_i \tag{5}$$

$$-\lambda \frac{\partial T(0,t)}{\partial y} = \alpha_f \left(T_{aw} - T(0,t)\right) \tag{6}$$

In the experiments a complication was introduced, since a true step change of the coolant temperature was not possible due to heat exchange in the supply tubing and plenum chamber. Thus, the adiabatic wall temperature became a function of time, which had to be accounted for in the evaluation. The measured coolant temperature distribution was approximated by a power series of the following form,

$$T_{tc}(t) = \sum_{n=0}^{N} A_n \frac{t^n}{\Gamma(n+1)} \tag{7}$$

usually chosen of 4th to 5th order.

Using this closed expression for T_{tc}, an analytical solution of the equations (3) to (7) was obtained for y=0 (Drost et al., 1997) using the Laplace transform method,

$$T_w - T_i = \left(T_{tg} - \eta T_{tg} - T_i\right)\left[1 - e^{\beta^2}\operatorname{erfc}(\beta)\right] - \eta \sum_{n=0}^{N}\left\{A_n\left(\frac{\kappa}{\alpha_f}\right)^{2n}\left[e^{\beta^2}\operatorname{erfc}(\beta) - \sum_{\tau=0}^{2n}\left([-2\beta]^\tau i^\tau \operatorname{erfc}(0)\right)\right]\right\} \tag{8}$$

with

$$\kappa = \frac{\lambda}{\sqrt{\Lambda}} = \sqrt{\rho \cdot \lambda \cdot c_p}$$

$$\beta = \frac{\alpha_f \sqrt{t}}{\kappa}$$

Eq. (8) contains the two unknowns α_f and η, which are deduced via a regression analysis. Least squares fitting of the model equation to the wall temperature rise yields the two unknowns. In theory two points of the temperature history would be sufficient to determine the two unknowns at each point of the surface. However, the measurement uncertainty can be significantly reduced by adding additional points to the evaluation and by applying regression analysis.

In the present work, a single layer of narrow-band liquid crystal with a bandwidth of 1K was used. Usually 5 to 6 tests were carried out at identical flow conditions but different coolant temperatures, while the freestream temperature was held constant. These test ensembles were then evaluated together by fitting eq. (8) through the measured points using a least squares regression procedure. For these variations, blowing rate, momentum flux and density ratio were kept approximately constant within ±3%. The range of coolant temperatures covered for each blowing rate was small compared with the general level of the cooling air temperature, i.e. $(T_{c,max}-T_{c,min})/T_{c,mean} < 0.1$.

The density ratio of approximately 1.65 was obtained with the use of foreign gas injection using CO_2, as proposed by Teekaram et al. (1989). For the definition of the Nusselt number the thermal conductivity of air was used, being based on the Eckardt temperature as defined in Kays and Crawford (1993).

Measurement Uncertainties

The uncertainty analysis for the regression method was carried out in two steps. A statistical analysis was conducted by systematically varying the number of tests of an evaluation ensemble. Here, the decrease of average relative deviations in η and α_f was observed with increasing test numbers. For more than 5 tests, this deviation fell below 1% so that the ensembles were considered to be in statistical equilibrium.

An uncertainty analysis according to Kline and McClintock (1953) was then carried out using the governing least squares equation derived from eq. (8). Uncertainty in heat transfer coefficient yields a rather constant value of 6%, and in local effectiveness a value of 10% at η=0.1, decreasing to 4% for η=0.3. For the latter case, uncertainty of laterally averaged effectiveness yields a value of 8%. The effect of the transient coolant temperature distribution during the tests with respect to evaluations conducted at constant average coolant temperatures was assessed to be up to 8% for the heat transfer coefficient and up to 16% for η. Further details on the uncertainty analysis are given in Drost et al. (1997).

The effect of lateral conduction within the cylinder in the vicinity of the cooling holes has been investigated with a finite-difference calculation (Hoffs, 1996). It was confirmed that the assumption of a semi-infinite material is still valid for a small region inbetween the cooling holes, for the present testing times. This can be explained with the ratios of the hole distances to the model wall thickness, which are close to two. In addition, the calculation showed that the influence of the heat exchange between the injected coolant and the hole walls on the coolant exit centerline temperature was negligible for a hole length-to-diameter ratio below five. These findings agree with results obtained by Forth et al. (1985) who verified the hole exit temperature using extremely fine thermocouples. For the tests it was always ensured that the time delay associated with the cylinder insertion and stabilisation of the flow was small compared to the timescale of the response of the cylinder wall temperature. This was done by adjusting the initial temperature of the measurement section to obtain response time above 1s.

Measurement Technique

The present image processing system is based on the hue capturing technique using an automated image processing system. Since the colour play of the liquid crystals is always taken under a certain angle with respect to the airfoil surface the original surface coordinates are correlated numerically with the camera picture. Calibration of the liquid crystals was always performed in situ at very low flow velocity to achieve thermal equilibrium of the model.

The application of the liquid crystals to the airfoil surface was done with a precision airbrush. Various measurements of surface roughness have been conducted with a Perthen SP6 profilometer and a piezo-electrique measuring sensor, which were essentially constant for the present measurements, as the surface was polished. Averaged roughness values are given by,

$$R_z = 12\,\mu m; \quad R_t = 16\,\mu m; \quad R_a = 2.5\,\mu m$$

An effect of surface roughness should only be present in the turbulent boundary layer downstream of the cooling holes. A calculation of the local roughness Reynolds number for the four-row configuration shows that a critical value of Re_k=5 is only obtained at an angle of φ=70° —thus the effect of surface roughness is considered negligible.

RESULTS/DISCUSSION HEAT TRANSFER

Overview of measurements

Table 2 contains the row-averaged cooling parameters for showerhead tests on the cylinder, based on approach conditions. Higher uncertainty is associated with the lowest blowing rate of 0.4, as the discharge coefficient was not constant for the different rows. As the injection temperature varied as a function of time due to heat pickup in the supply chamber, the data was averaged over 10s. Care was taken regarding the exact positioning of the stagnation point with respect to the mainflow direction, which was essential for the three-row configuration with one cooling row along the stagnation line. The Reynolds number is based on approach conditions and cylinder diameter.

Three-Row Configuration				Four-Row Configuration			
AoA	G	I	CD	AoA	G	I	CD
0°	0.43	0.14	0.52	0°	0.44	0.15	0.67
	0.87	0.46	0.71		0.88	0.46	0.89
	1.39	1.14	0.77		1.36	1.07	0.93
	1.78	1.69	0.80		1.81	1.91	0.93
-10.5°	0.43	0.17	0.50	-14°	0.43	0.22	0.51
	0.88	0.48	0.71		0.88	0.52	0.83
	1.41	1.18	0.76		1.36	1.12	0.90
	1.80	1.90	0.79		1.82	1.93	0.92
+10.5°	0.42	0.17	0.49	+14°	0.43	0.22	0.56
	0.88	0.48	0.72		0.87	0.49	0.86
	1.41	1.17	0.77		1.33	1.07	0.89
	1.81	1.91	0.80		1.77	1.84	0.92

Table 2 Overview Measurements

Pressure measurements have been performed on several spanwise positions indicating a good uniformity of the flow field, which is shown for the 3-row configuration in Fig. 3. Also the velocity distribution is displayed for both configurations for the stagnation region.

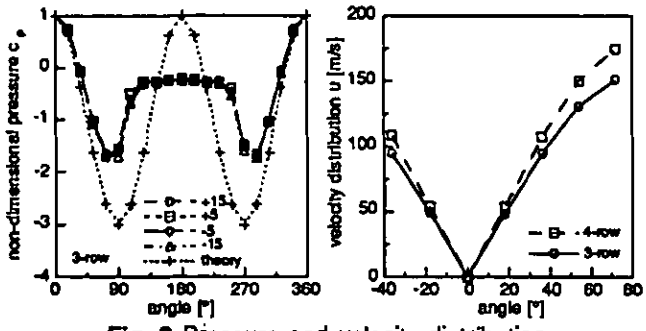

Fig. 3 Pressure and velocity distribution

Heat transfer without cooling

Heat transfer measurements without cooling have been conducted for the two cases on a model without holes, in order to show the feasibility of the new insertion mechanism and to obtain baseline conditions (Fig. 4). The non-dimensionalized heat transfer is identical since the Mach number effect is negligible. High heat transfer with $Nu/Re^{0.5}$ of 1.3 can be observed at the stagnation point, showing a good symmetric behaviour. The boundary layer stays laminar to φ=80°, and heat transfer decreases almost linear. The results compare well with a stagnation point correlation of Dullenkopf and Mayle (1995), with a dimensionless strain rate being calculated to a_1=3.5.

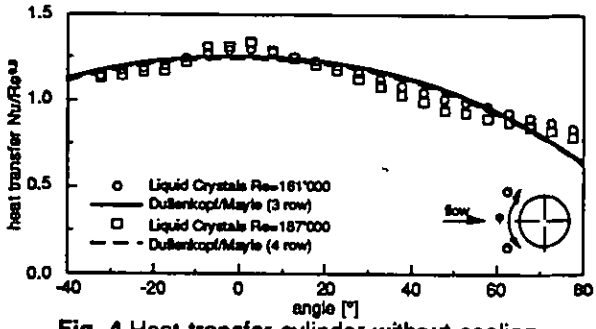

Fig. 4 Heat transfer cylinder without cooling

Discharge coefficients

The hole discharge coefficients for the single rows were determined from the measured total coolant massflow and a calculated ideal massflow, assuming isentropic compressible flow. In this calculation the effect of static outer pressure was taken into account, but not the effects of crossflow which could not be assessed separately. For the three higher blowing rates with hole pressure ratios p_p/p_g above 1.02 (Fig. 5) constant discharge coefficients were assumed. For the lowest blowing rate of 0.4 the discharge coefficients for one or two rows had to be extrapolated, while one row was usually above the limiting pressure ratio value. The product of row discharge coefficient and theoretical row massflow was then used to calculate the hole exit velocity, and subsequently blowing rate, momentum flux ratio and coolant hole Reynolds number were determined. Above a coolant Reynolds number of 4500 the discharge coefficient is constant, thus being only a function of the hole pressure ratio.

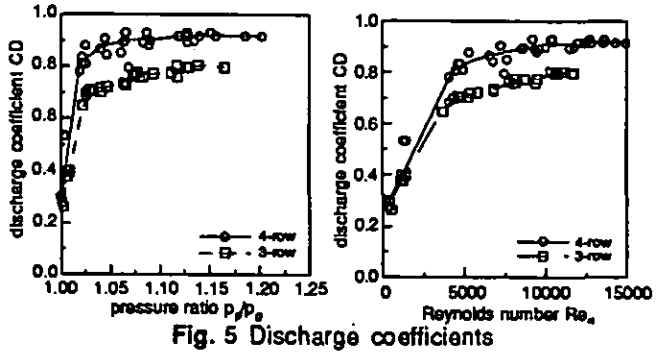

Fig. 5 Discharge coefficients

Spanwise effectiveness distribution

Two-dimensional contour plots are only presented for the zero incidence to show the good spanwise symmetry (Fig. 6). The spanwise effectiveness distributions are presented in steps of 0.1 for the two cooling configurations, at a blowing rate of G=0.9. The injection patterns are remarkably homogenous for all tests. The mixing process is accomplished earlier with the four-row configuration in comparison to the three-row configuration, which is probably due to the stronger effect of the double row injection, in combination with a 60% higher massflow.

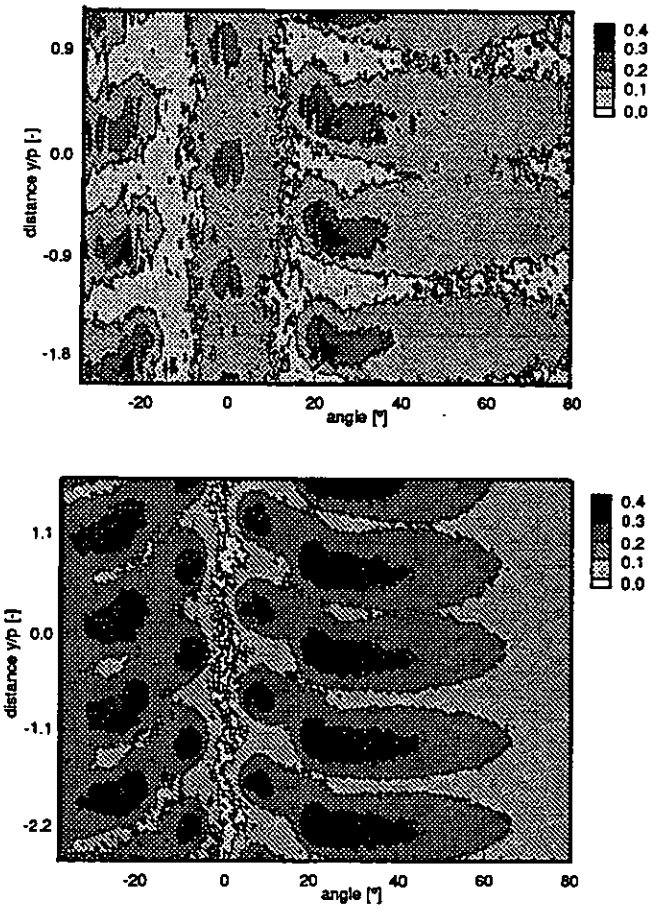

Fig. 6 Effectiveness at zero incidence for G=0.9

Averaged effectiveness and heat transfer

The results of the investigation are presented in form of spanwise averaged graphs containing the cooling effectiveness and the heat transfer, the latter being non-dimensionalised, as a function of all four blowing rates (Fig. 7-12). The peaks observed at the injection locations result from the averaging process, which takes only the space in between the holes (in spanwise direction) into account, and should thus not be considered as realistic data points. For a small region in between the holes the measurement results are still valid, while care has to be taken regarding interpretation of the near hole region due to heat exchange from the hole. In the following, only the region downstream of the cooling rows is discussed. For positive and negative incidences two independent measurement series had to be performed, due to the camera viewing angle which covered about -20° to +80°.

Zero incidence

For the three-row configuration at zero indicence (Fig. 7) the highest effectiveness is obtained at the lowest blowing rate of 0.4 with η=0.26, which decreases to 0.17 further downstream. A much lower effectiveness is seen for the blowing rate of 0.9 with a maximum value of 0.16 just behind the holes. The two higher blowing rates are similar, showing rather low effectiveness of 0.10 at φ=80°. Heat transfer behind the holes is highest for the low blowing rate of 0.4 with $Nu/Re^{0.5}$=2.2, while the maximum for the other blowing rates is almost identical with a value of 1.8. At a position of φ=80° heat transfer is about 1.0, being about 25% higher than for the uncooled case.

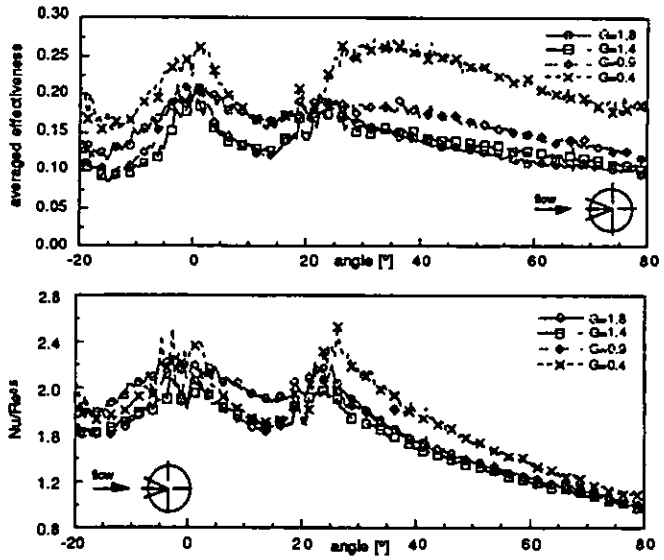

Fig. 7 Zero incidence for 3-row configuration

Also for the four-row configuration at zero incidence (Fig. 8), it can be seen that the lowest blowing rate of 0.4 has the best cooling characteristics behind the holes with η=0.30, decreasing strongly to η=0.14. Here, the blowing rate of 0.9 shows a similar behaviour but does not decrease as much. A maximum effectiveness of 0.25 is observed for the blowing rate of 1.4, which decreases less rapidly than the previous case, so that the curves overlap further downstream. The highest blowing rate of 1.8 shows the lowest effectiveness with 0.19, but remains almost constant. Regarding the heat transfer, it can be seen that the lowest blowing rate causes the highest values with 2.5 behind the holes, while the higher blowing rates stay below this value. At about φ=55° an intersection of the curves is observed, and this trend is reversed.

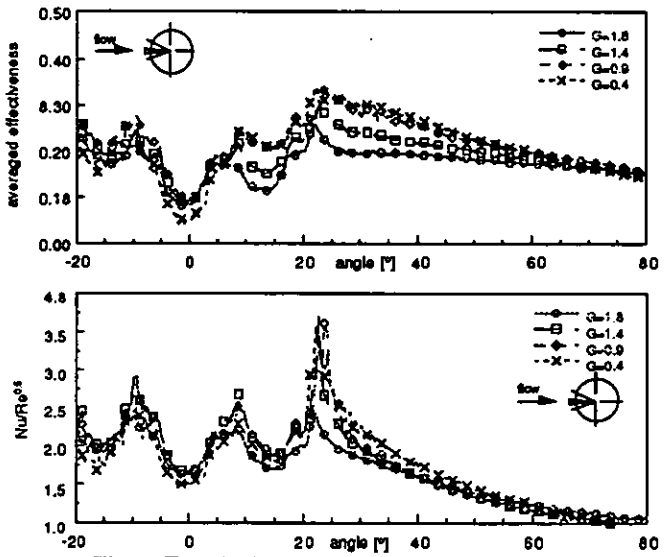

Fig. 8 Zero incidence for 4-row configuration

Negative incidence

For the three-row configuration at a negative incidence of 10.5° (Fig. 9), the coolant which is ejected at the stagnation point is completely blown onto the second row further downstream. This results in quite high effectiveness for the low blowing rate of 0.4 with η=0.28 behind the holes and η=0.16 at φ=80°. Similarly to the zero incidence, it can be seen that the next higher blowing rate of 0.9 achieves a quite good effectiveness of 0.21. The effectiveness for the two higher blowing rates have a rather flat characteristics, with η=0.16 for G=1.4 and η=0.12 for G=1.8. Heat transfer for the low blowing rate is highest with a value of 2.4 behind the holes, while the blowing rate of 0.9 is at $Nu/Re^{0.5}$=1.9. The heat transfer for the two higher blowing rates is identical, and shows lower values compared to the zero incidence.

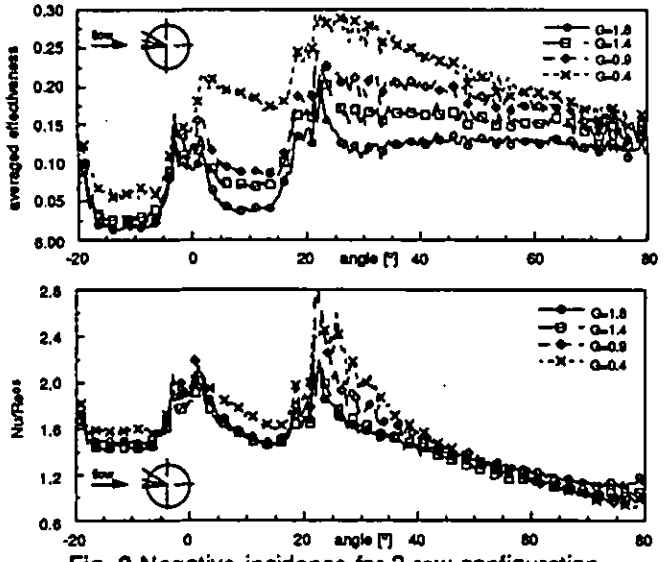

Fig. 9 Negative incidence for 3-row configuration

Negative incidence for the four-row configuration (Fig. 10) results also in high cooling effectiveness in comparison to zero incidence, but here the highest effectiveness of 0.48 is seen for the blowing rate of 1.4. Subsequently, the blowing rate of 1.4 decreases steeply to η=0.20, which corresponds approximately to the values for the other blowing rates. Unlike to the previous observations, the blowing rate of 0.4 ranks only third with an effectiveness of 0.35. Effectiveness for the high blowing rate of 1.8 is again lowest at η=0.30. At an angle of φ=75° a slight increase in effectiveness can be observed, which may be caused by separation and can more clearly be seen for the heat transfer. Here, the blowing rate of 1.4 shows extremely high values with $Nu/Re^{0.5}$=3.5. The three other blowing rates are almost identical, and show lower heat transfer with a maximum of $Nu/Re^{0.5}$=2.1 behind the holes.

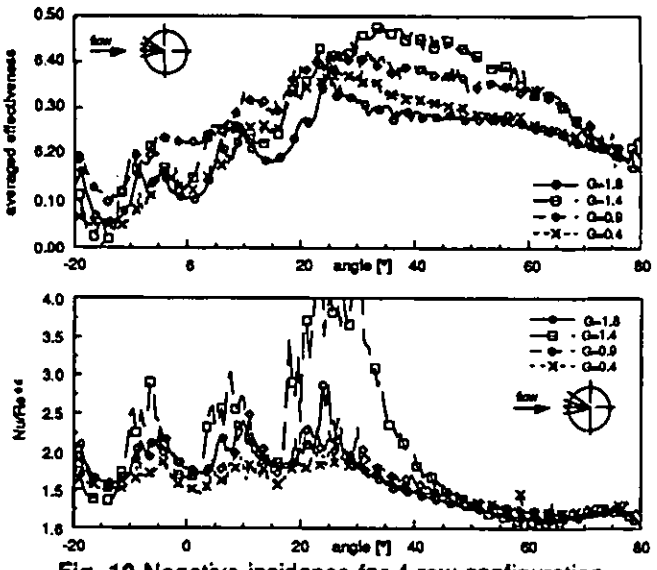

Fig. 10 Negative incidence for 4-row configuration

Positive incidence

Rather low effectiveness is obtained for all blowing rates at a positive incidence for the three-row configuration (Fig. 11), as only one cooling row is effective. The low blowing rate shows the best effectiveness immediately behind the holes —but rapidly decreases further downstream to almost zero at φ=80°. The blowing rate of 0.9 shows a value of η=0.11 behind the holes, with moderate decrease to η=0.06. The two higher blowing rates are almost identical with a flat characteristics (as observed for negative incidence) and an effectiveness of 0.05. In comparison to zero and negative incidence, heat transfer is considerably lower and all blowing rates show similar values of 1.6 behind the holes, decreasing to 1.0.

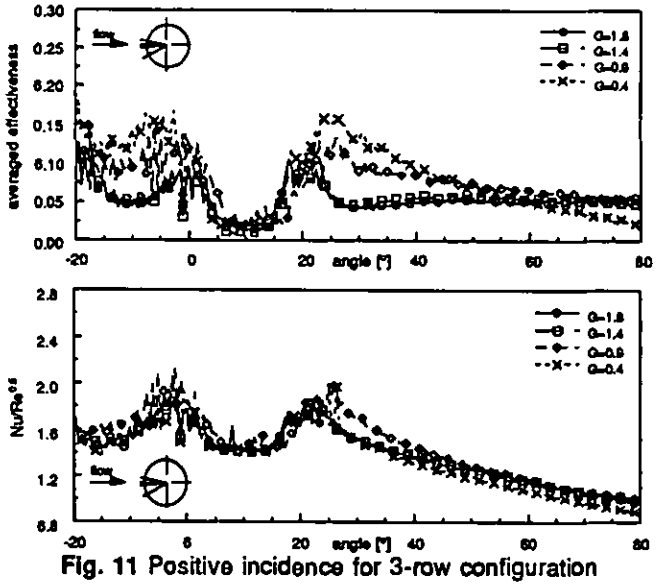

Fig. 11 Positive incidence for 3-row configuration

For the four-row configuration at a positive incidence (Fig. 12)—also with only one protective cooling row—the best effectiveness is obtained with the blowing rate of 0.9 to η=0.24. Although a steep decrease is observed the

effectiveness remains highest at a value of η=0.10. The low blowing rate of G=0.4 has quite poor cooling behaviour with an effectiveness close to zero at φ=80°. While the blowing rate of G=1.4 has a rather flat characteristics with about η=0.10, the highest blowing rate of G=1.8 has poor cooling behind the holes, but shows increased effectiveness further downstream which may be explained with lift-off and subsequent re-attachment. The heat transfer results indicate quite high values for the blowing rate of 0.9 with $Nu/Re^{0.5}$=2.2 behind the holes. The blowing rates of 1.4 and 1.8 are almost identical and show lower values. Heat transfer for the lowest blowing rate is extremely low—it is almost comparable to the case without cooling.

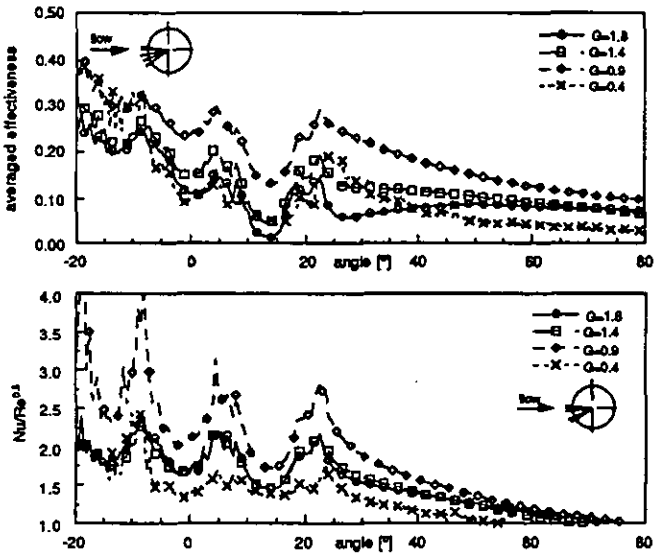

Fig. 12 Positive incidence for 4-row configuration

CONCLUSIONS

An investigation of cooling effectiveness and heat transfer on a showerhead-cooled cylinder was conducted for a three- and four-row cooling configuration at zero and off-design incidences, using the transient liquid crystal technique.

At zero incidence it could be observed for both configurations that a blowing rate of 0.4 resulted in the highest effectiveness of approximately 0.3, with slightly higher values for the four-row configuration. Associated heat transfer was also highest for this blowing rate, being in the order of $Nu/Re^{0.5}$=2.5. Poor cooling behaviour was seen for a blowing rate of 1.8 with an effectiveness below 0.2.

Negative incidence for the three-row configuration showed a similar trend—in comparison to the zero incidence—with a larger scatter of the blowing rates. For the four-row configuration much higher effectivaness was observed, being as high as 0.5 for a blowing rate of 0.9, while heat transfer was as elevated as $Nu/Re^{0.5}$=3.5.

A strong decrease in effectiveness was observed for the low blowing rate of 0.4 at positive incidence—with a peak just behind injection for the three-row configuration. Here, highest effectiveness was in general achieved with a blowing rate of 0.9. Again, the highest blowing rate showed poor cooling behaviour, which was probably due to lift-off behind the holes.

A comparison between the two configurations showed much higher effectiveness—but also increased heat transfer—for the four-row configuration, with a 60% higher massflow.

ACKNOWLEDGEMENTS

The research project is subsidized by ABB, Baden, Switzerland and the "Commission pour l'encouragement de la recherche scientifique" (CERS-KWF), Switzerland. The authors are very grateful to Mr. B. Weigand for his revision of the paper.

REFERENCES

Camci, C. and Arts, T., 1990
An Experimental Convective Heat Transfer Investigation Around a Film-Cooled Gas Turbine Blade.
Journal of Turbomachinery, Vol. 112, pp. 497-503
Drost, U., Hoffs, A. and Bölcs, A., 1997
Utilization of the Transient Liquid Crystal Technique for Film Cooling Effectiveness and Heat Transfer Investigations on a Flat Plate and a Turbine Airfoil.
proposed for publication ASME 97, Orlando
Dullenkopf, K. and Mayle, R.E., 1995
An Account of Free-Stream-Turbulence Length Scale on Laminar Heat Transfer.
Journal of Turbomachinery, Vol. 117, pp. 401-406
Forth, C.J.P., Loftus, P.J. and Jones, T.V., 1985
The Effect of Density Ratio on the Film Cooling of a Flat Plate.
AGARD Conference Proceedings No. 390, Bergen
Häring, M., Hoffs, A., Bölcs, A. and Weigand, B., 1995
An Experimental Sudy to Compare the Naphthalene Sublimation with the Liquid Crystal Technique in Compressible Flow.
ASME Paper 95-GT-16, Houston
Hoffs, A. 1996
Experimental Investigations of Heat Transfer and Film Cooling Effectiveness using the Transient Liquid Crystal Technique.
Ph.D. Thesis No. 1510, Swiss Federal Institute of Technology-Lausanne (EPFL)
Kami, J. and Goldstein, R.J., 1990
Surface Injection Effect on Mass Transfer From a Cylinder in Crossflow: A Simulation of Film Cooling in the Leading Edge Region of a Turbine Blade.
Journal of Turbomachinery, Vol. 112, pp. 418-427
Kays, W.M. and Crawford, M.E., 1993
Convective Heat and Mass Transfer.
McGraw Hill, Inc., New York, 3rd ed.
Kline, S.J. and McClintock, F.A., 1953
Describing Uncertainties in Single Sample Experiments.
Mechanical Engineering, January 1953
Mayle, R.E. and Anderson, A., 1989
Velocity and Temperature Profiles for Stagnation Film Cooling.
Heat Transfer in Gas Turbine Engines, HTD Vol. 120, pp. 51-57
Mehendale, A.B. and Han, J.C., 1990
Influence of High Mainstream Turbulence on Leading Edge Film Cooling Heat Transfer.
ASME paper 90-GT-09, accepted for publication in the Transactions
Mick, W.J. and Mayle, R.E., 1988
Stagnation Film Cooling and Heat Transfer, Including its Effect Within the Hole Pattern.
Journal of Turbomachinery, Vol. 110, pp. 66-72
Salcudean, M., Gartshore, I., Zhang, K. and McLean, I., 1994
An Experimental Study of Film Cooling Effectiveness Near the Leading Edge of a Turbine Blade.
Journal of Turbomachinery, Vol. 116, pp. 71-79
Teekaram, A.J.H., Forth, C.J.P., and Jones, T.V., 1989
The Use of Foreign Gas to Simulate the Effects of Density Ratios in Film Cooling.
Journal of Turbomachinery, Vol. 111, pp. 57-62
Teekaram, A.J.H., Forth, C.J.P. and Jones, T.V., 1990
Film Cooling in the Presence of Mainstream Pressure Gradients.
ASME Paper 90-GT-334
Vedula, R.,J. and Metzger, D.E., 1991
A Method for the Simultaneous Determination of Local Effectiveness and Heat Transfer Distributions in Three-Temperature Convection Situations.
ASME Paper 91-GT-345, Orlando